Appl. Phys. B 55, 126–131 (1992)

Applied Physics B Photophysics and Laser Chemistry

Measuring Chaotic Scenarios in a Sodium-Filled Resonator

M. Möller and W. Lange

Institut für Angewandte Physik, Westfälische Wilhelms-Universität, Corrensstrasse 2/4, W-4400 Münster, Fed. Rep. Germany

Received 3 February 1992/Accepted 12 March 1992

Abstract. A sodium-filled Fabry-Perot resonator shows many different types of irregular behavior. A sophisticated experimental apparatus allows reproducible measurements of oscillation scenarios leading to chaos and thus permits a detailed classification of the different phenomena. A quantitative explanation – featuring a new mechanism – for the best reproducible class of chaotic oscillations is given.

PACS: 42.50.Tj, 42.65.Pc

Nonlinear resonators, i.e., resonators containing a nonlinear optical medium, are an important class of systems for studying chaos in optics. They feature a combination of an optical nonlinearity and a feedback provided by the resonator. In order to study their behavior it is necessary to understand both the microscopic behaviour under the influence of the light field and the effects of the resonator. The system we study is a Fabry-Perot resonator filled with sodium vapor that is known to show self-oscillations due to spin precession in the ground state under the influence of a static magnetic field [1]. These oscillations can become chaotic if the magnetic field is not perpendicular to the optical axis [3, 4]. In this paper, we show the experimental requirements for reproducible measurements on this system and discuss the parameter ranges where agreement with the model can be expected.

1 Theoretical Description

1.1 Microscopic Model

In [1] the theoretical model describing the behavior of spin-$\frac{1}{2}$ atoms in a static magnetic field under conditions of strong pressure broadening was presented in detail. Starting from the density matrix formalism, the final set of equations was obtained using adiabatic elimination techniques. The dynamical variables are $\mathbf{m} = (u, v, w)$, the expectation values of the Cartesian components (x, y, z) of the spin in the sample, and, as introduced in [2], the population s of the excited state. The quantization axis $\hat{e}_z$ is defined by the direction of the laser beam. In their most generalized form, the equations of motion are

$$\dot{\mathbf{m}} = -\gamma_{\text{eff}}\mathbf{m} + \mathbf{\Omega}_{\text{eff}} \times \mathbf{m} + \mathscr{D}\hat{e}_z\,, \tag{1a}$$

$$\dot{s} = -\Gamma_{\text{eff}}s + \mathscr{S} - \mathscr{D}w\,, \tag{1b}$$

$$\mathscr{S} = P_- + P_+, \qquad \mathscr{D} = P_- - P_+\,. \tag{1c}$$

Here P_+ and P_- represent the pump rates due to the σ_+ and σ_- light, respectively, inside the resonator, $\mathbf{\Omega}_{\text{eff}}$ is the effective Larmor frequency, γ_{eff} and Γ_{eff} are the effective decay constants of the ground state orientation and the excited state population, respectively. Generally, the effective quantities are functions of $P_\pm$, w and s. Equation (1a) describes the precession of $\mathbf{m}$ around the direction of the effective magnetic field with angular frequency $|\mathbf{\Omega}_{\text{eff}}|$, with the driving terms being proportional to the difference between the two pump rates and the damping terms γ_{eff}. Equation (1b) describes the excitation due to the light field which decays with Γ_{eff} and includes the dependence on the longitudinal orientation component w.

1.2 Resonator

The feedback in the system under study is provided by a Fabry-Perot resonator. Assuming the resonator time constant to be small compared to the relaxation rates of the medium, the electric field can be eliminated adiabatically. Thus, the influence of the resonator on the pump rates is described by the Airy function

$$P_\pm = P_{0,\pm}\,\mathrm{Ay}(R, R_\pm, \varphi_\pm)\,, \tag{2}$$

$$\mathrm{Ay}(R, R_\pm, \varphi_\pm) = \frac{1-R}{1+R_\pm^2 - 2R_\pm\cos(\varphi_\pm)}, \tag{3}$$

$P_{0,\pm}$ being the pump rates that would be present without a resonator. Apart from the mirror reflectance R, this function depends on the cavity detuning, the absorption coefficient $\alpha_\pm$, and the refractive index $n_\pm$ (for $\sigma_\pm$ light, respectively), the latter two being linear functions of w and s

$$\alpha_\pm(w,s) = \alpha_0(1 \pm w - 2s)\,, \tag{4a}$$

$$n_\pm(w,s) = 1 + (n_0 - 1)(1 \pm w - 2s)\,. \tag{4b}$$

Here, α_0 and n_0 are the values of the absorption coefficient and the refractive index for the actual light frequency in the absence of nonlinear effects. Working in a chiefly dispersive regime we can neglect the dependence on $\alpha_\pm$

$$R_\pm = R\exp(-\alpha_\pm L_{\exp}) \approx R\exp(-\alpha_0 L_{\exp}) \tag{5}$$

and thus, the argument of the Airy function is

$$\varphi_\pm(w,s) = \frac{2\pi L_{\exp} n_\pm(w,s)}{\lambda} = \varphi_0 + \varphi_{nl,\pm}(w,s)\,, \tag{6}$$

$$\varphi_0 \equiv \frac{2\pi L_{exp} n_0}{\lambda}\,. \tag{7}$$

It has to be emphasized that no spatial dependences are included in this model, i.e., the light field is assumed to be a plane wave interacting with a uniformly distributed nonlinear medium.

1.3 Control Parameters

In our experiments we use only σ_+ polarized light, and thus, in the following discussions only the "+"-indexed quantities will appear. As can be seen from (1a) and (1b), the important parameters in this system are the magnetic field and the pump rate inside the resonator. This rate depends on the laser power, measured in terms of P_0, and on the detuning of the *linear* resonator φ_0:

$$P(w,s) = P_0\left[\mathrm{Ay}(\varphi_0) + \varphi_{nl}(w,s)\frac{\partial\,\mathrm{Ay}}{d\varphi}\bigg|_{\varphi_0} + \ldots\right]. \tag{8}$$

Thus φ_0, referred to as *resonator phase shift* in this article, determines the pump rate in the absence of nonlinear effects – via the local magnitude of the resonance function – and the *coupling strength* of the nonlinear feedback – via the local slope.

2 Experimental Setup

The nonlinear resonator we use consists of a heated quartz tube containing a small quantity of solid sodium in an argon atmosphere of about 200 mbar, sealed by identical mirrors forming a symmetric confocal resonator with a length of 150 ± 1 mm (Fig. 1). The resonator has a free spectral range (FSR) of 1 GHz and a finesse of about 30, including linear absorption. The magnetic field is created by three pairs of Helmholtz coils. The laser light is provided by an argon-ion laser pumped ring dye laser with a built-in stabilization (Spectra Physics *Stabilok*) (Fig. 2). The laser was operated at a frequency of about 90 GHz above the atomic resonance, with a power of about 150 mW in front of the resonator.

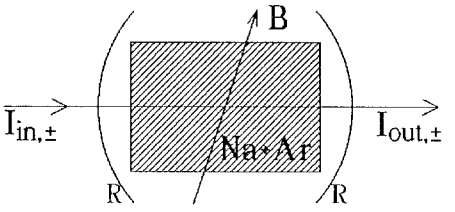

Fig. 1. Schematic experimental setup

The transmitted intensity is recorded by a digital storage oscilloscope controlled by a microcomputer.

The resonator phase φ_0 has to be controlled with very high precision because of the sensitive dependence of P on φ_0. Given the resonator parameters mentioned above, unwanted phase fluctuations should be small compared to $2\pi/30$. On the other hand, being a control parameter, φ_0 should be able to be varied over a range of 2π. It is thus crucial for the experiment that both these requirements are met simultaneously.

2.1 Phase Stabilization

As seen in (7), φ_0 is the ratio of the resonator length and the dye laser wavelength. For φ_0 to remain constant, both have to be stabilized simultaneously to the same reference, in order to avoid a relative drift. The reference we use is a stabilized helium-neon laser. The experimental resonator and an additional confocal reference resonator with a FSR of 750 MHz are stabilized to the helium-neon wavelength. The stability of the dye laser relative to the reference resonator is monitored using the polarization stabilization scheme described by Hänsch et al. [6]. Any deviations due to drift are fed back to the Stabilok reference cavity, thus locking the dye laser frequency to the helium-neon reference as well. The stabilities obtained in the individual regulation loops are:

reference rel. to He–Ne laser: 0.5 MHz
experiment rel. to He–Ne laser: 2.5 MHz
dye laser rel. to reference: 2.0 MHz.

They imply a worst case instability of φ_0 of 1/200 of the free spectral range of the experimental resonator.

2.2 Phase Variation – The "Optical Vernier"

By using the described stabilization scheme, with all stabilization loops locked, the experiment and reference resonator lengths will be integer multiples of the helium-neon wavelength, while the dye laser wavelength will be an integer fraction of the reference resonator length:

$$\begin{aligned} L_{\exp} &= N_1\,\lambda_{\mathrm{ref}}\,,\\ L_{\mathrm{ref}} &= N_2\,\lambda_{\mathrm{ref}}\,,\\ L_{\mathrm{ref}} &= N_3\,\lambda_{\mathrm{dye}}\,,\\ \frac{L_{\exp}}{\lambda_{\mathrm{dye}}} &= \frac{\varphi_0}{2\pi} = \frac{N_1 N_3}{N_2}\,. \end{aligned} \tag{9}$$

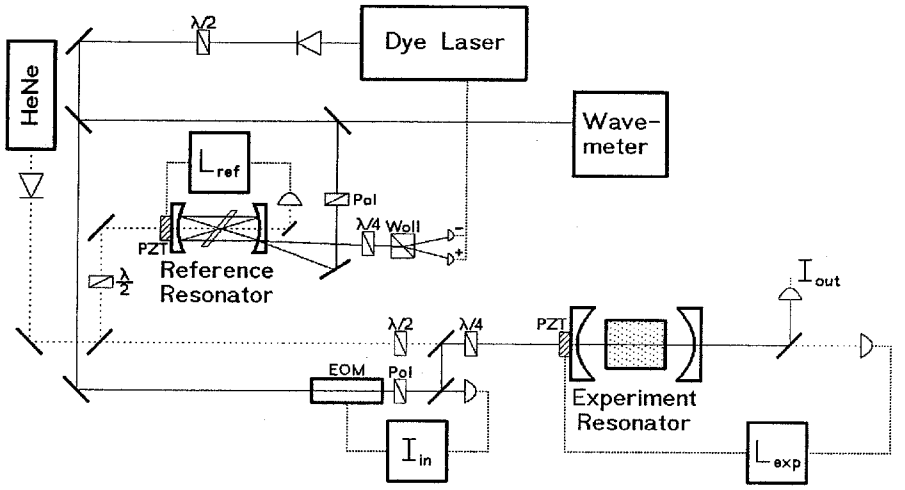

Fig. 2. Detailed experimental setup. Abbreviations: *EOM* electro-optical modulator, *Woll* Wollaston prism, *Pol* polarizer, $\lambda/2$ halfwave plate, $\lambda/4$ quarterwave plate, *PZT* piezo translator; the diode symbols denote optical isolators. Vacuum systems, heating and Helmholtz coils are not shown

Here, L_{exp} and L_{ref} denote the round-trip lengths of the experiment and reference resonators. The exact values of the integers N_1, N_2 and N_3 can obviously not be controlled. Thus, in the worst case, the phase might be perfectly stabilized at a value separated by π from the value desired. A small amount of fine tuning is possible by shifting the working point of the reference length stabilization, but certainly not over half a FSR. The only other possible variation is a shift to an adjacent resonance – changing the frequency by a full FSR.

A method was developed to perform arbitrary phase changes without having to leave the locked state of the stabilization. As it is based on the principle of a vernier scale such as that on a (metric) slide caliper, we introduce it as the *optical vernier*. Without making use of the vernier scale, only lengths of m millimeters, m integer, can be measured exactly by aligning the zero line of the vernier scale with one of the lines on the main scale that are equally spaced by one millimeter. Using the vernier scale, one looks for the coincidence of a line at a distance of $9n/10\,\text{mm}$ from the zero line on the vernier scale with the $(m+n)$th line on the main scale, thus being able to exactly measure a length of $m.n$ millimeters.

Here, the ratio of the different line spacings corresponds to that of the helium-neon and the dye laser wavelengths, being approximately 15/14. A change from one stabilized state in the reference resonator (with a FSR of ν_{ref})

$$L_{\text{ref}} = m \cdot \lambda_{\text{dye}} \Longleftrightarrow \nu_{\text{dye}} = m \cdot \nu_{\text{ref}} \tag{10}$$

to an adjacent resonance for *both* the length stabilization and the dye laser stabilization is analogous to the comparison of adjacent lines on both scales of a caliper:

$$\begin{aligned} L_{\text{ref}} &\rightarrow L_{\text{ref}} + \lambda_{\text{ref}} = (m+1)\,\lambda_{\text{dye}}\,, \\ \nu_{\text{dye}} &\rightarrow \nu_{\text{ref}} \left[m - \frac{\lambda_{\text{ref}} - \lambda_{\text{dye}}}{\lambda_{\text{dye}}} \right], \\ \nu_{\text{dye}} &\rightarrow \nu_{\text{dye}} - \nu_{\text{ref}} \frac{\lambda_{\text{ref}} - \lambda_{\text{dye}}}{\lambda_{\text{dye}}}\,. \end{aligned} \tag{11}$$

With the approximation given above, this leads to a frequency skip of approximately 1/14 of FSR of the reference resonator, i.e., approximately 50 MHz.

Technically, jumping to adjacent resonances is achieved by applying a fast voltage step to the PZT driver circuit, resulting in a sudden length change of the reference resonator of approximately one helium-neon wavelength. Subsequently the exact resonator length will be attained by the length stabilization circuit that did not notice the fast change to the same working point on another resonance. Finally, since the locking to the Stabilok works slowly, the Stabilok reference will finally be adjusted to provide the matching dye laser wavelength. The procedure can be repeated in both directions, limited only by the adjustment range of the PZT. Here, the full FSR of the nonlinear resonator (1 GHz) can be covered by a variation of the reference resonator mirror spacing of 20/4 helium-neon wavelengths ($\approx 3.1\,\mu\text{m}$). This, together with the fine tuning mentioned before, makes it possible to adjust to any desired phase. Thus we are able to trace any phase-dependent scenario over its full range without the restriction of repetitive phase scans. This includes the possibility to reproduce large phase changes in both directions in order to study hysteresis loops as well as to perform phase stabilized measurements of a particular oscillatory behavior.

3 Experimental Results

3.1 Phase Scans – Generalized Bistability

As a first step in a series of measurements we look at the behavior during a *phase scan* in order to have an overview of phase-dependent changes. As can be seen from Fig. 3, an obvious hysteresis loop can be observed: While increasing the phase from values far from resonance, a long sequence of quasiperiodic behavior is followed by periodic behavior and a period-doubling sequence into chaos. After that, the system will switch into a state of high transmissions, go through another sequence of oscillations and finally, switch to low transmission. If the phase is then decreased, the system will remain in the low transmission state for a wide phase range. It will not switch to higher transmission until the quasiperiodic regime is reached again. This kind of behavior can be called *generalized bistability*, as there is a phase range where a fixed point and a chaotic attractor coexist.

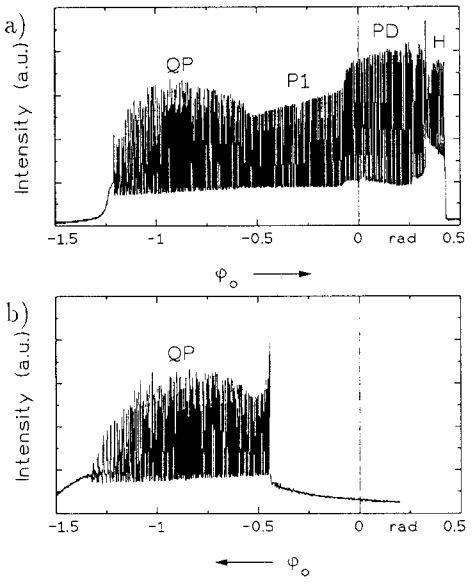

Fig. 3. a Increasing and **b** decreasing phase scan. The system passes through adjoining ranges of quasiperiodic (*QP*), simple periodic (*P1*) and period doubling (*PD*) behavior. In range *H* there are oscillations in a higher transverse resonator mode

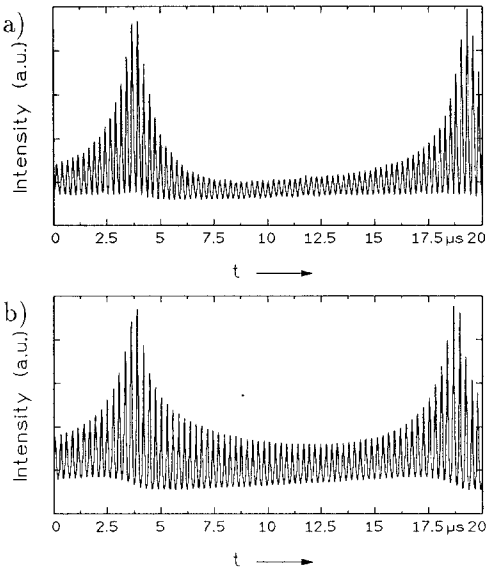

Fig. 4. a Measured and **b** simulated time series of quasiperiodic oscillation

As the hysteresis is not only present during fast phase changes, the oscillatory regime in the upper branch can only be reached via the proper *history* of phase variations using the vernier mechanism. Once the system has accidentally switched from the chaotic regime to the high transmission regime, in order to reproduce a measurement of a chaotic oscillation, one has to run through the whole loop again. Without such a possibility to reproduce and stabilize a specific phase value, it would only be possible to perform single-shot measurements of chaotic oscillations. It is doubtful whether large-scale evaluations of such measurements would produce very meaningful results.

3.2 Transverse Effects

In this experiment we cannot ignore the geometrical properties of laser beam and resonator. As opposed to what was assumed in the model, there are no plane waves and infinite plane mirrors, but a confocal resonator and a Gaussian beam mode-matched to the empty resonator. The transverse structure of the beam implies a transverse dependence of the dynamical variables and thus a transverse distribution of absorption and refractive index. As is shown by Nalik et al. [7] this leads to a change in the mode structure of the resonator. We observed that upon switching up to the higher transmitting state, mode switching occurs. The transverse structure in this state can be described as a superposition of low-order Gauss-Laguerre or Gauss-Hermite modes, which is very sensitive to deviations from an exactly mode-matched incoming Gaussian beam. As such deviations can occur with very small alignment inaccuracies of geometrical fluctuations in the laser jet, they are hardly measurable let alone reproducible. For that reason, we insert an aperture into the resonator to prevent premature mode switching and restrict our measurements to the region before the switching even though there are ranges of oscillatory and chaotic behavior in the high transmitting state as well.

3.3 Individual Oscillation Types

As can be seen from Fig. 3, there is a wide range of quasiperiodic (torus) oscillations. This starts from *heavy breathing*, goes through more or less nonlinear amplitude modulation with the modulation depth finally going to zero and ends up with a simple periodic signal. A typical example of this type is shown in Fig. 4a. Any oscillation in this region is temporally stable and can be observed over at least some minutes.

After going through a phase range of simple periodic oscillations with increasing amplitude, a period doubling sequence is reached that can be resolved up to period 4 and then enters chaos. Measurements in the chaotic range can be performed with rather good stability, though the sensitivity on phase changes is naturally much higher as in the quasiperiodic regime. Working close to the switching threshold may lead to accidental switching, but the parameter range can easily be regained with the procedure described above. About one hundred time series were recorded in the chaotic regime, one record containing 25,000 8-bit samples with 10 ns time resolution. A typical example of a chaotic oscillation is shown in Fig. 5a.

All types of oscillations could easily be reproduced an arbitrary number of times even after some hours or in another experimental session, being characterized using an on-line display of phase portrait and first-return map of a recorded time series. (The return map of the time series of Fig. 5a is shown in Fig. 6a.)

Nearly all the chaotic time series wer evaluated over their full length with an attractor dimension estimation program using the Grassberger-Procaccia algorithm [10]. The dimen-

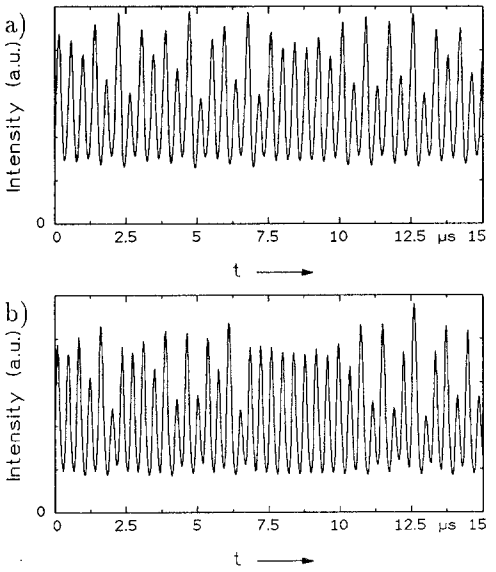

Fig. 5. **a** Measured and **b** simulated time series of chaos. Correlation dimensions are **a** 1.92, **b** 1.94

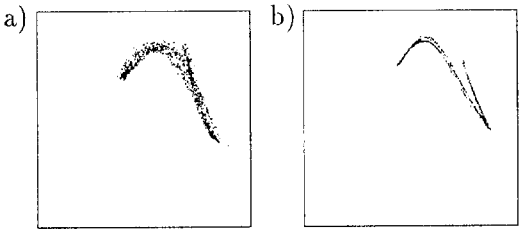

Fig. 6. **a** Measured and **b** simulated return maps of chaotic time series shown in Fig. 5

sion values covered a range from 1.55 to 2.25, mostly between 1.70 and 1.95, where similar dimension values corresponded to similar signal shapes, phase portraits and return maps. Estimations of Kolmogorov entropies were performed as well.

4 Comparison to the Model

4.1 Nonlinear Mechanisms

In our theoretical approach we consider two physical mechanisms that induce nonlinear couplings. One is the light-shift effect, that gives an additional contribution to the longitudinal component of the magnetic field Ω_z proportional to the laser detuning from the atomic resonance and to the difference $\mathscr{D}$ between the individual pump rates (see [1, 5]). The second mechanism was not considered in this context before; it is based on the effect of radiation trapping or radiation diffusion. This effect is known to counteract the build-up of a ground state orientation due to optical pumping [8]. As it is a diffusive effect, it is strongly dependent on the spatial structure of light field and excitation distribution [9]. Nevertheless, it is introduced here phenomenologically as a reabsorption of fluorescence with a spatially invariant probability leading to an additional incoherent pumping [11]. This adds a predominating contribution to the ground state relaxation rate γ_{eff} that oscillates with the excitation s. It also causes a prolongation of the lifetime of the excited state population, thus decreasing Γ_{eff}.

4.2 Numerical Results

The set of differential equations (1a) and (1b) was integrated using the Runge-Kutta algorithm. The parameters were calculated from the experimental parameters as far as possible or adapted to match experimentally observed dependences on parameter changes. The parameters that explicitly introduce frequencies, i.e., the Larmor frequencies, were exact. The results are:

- The nonlinear scenario, i.e., the sequence of different kinds of oscillatory behavior could be reproduced with similar individual phase ranges.
- The coexistence of fixed point and chaotic attractor (generalized bistability) was confirmed.
- Quasiperiodic oscillations could be reproduced both in the fundamental and in the modulation frequency (Fig. 4b).
- Chaotic oscillations could be reproduced both in oscillation frequency and modulation contrast (Fig. 5b) with similar looking return maps (Fig. 6b) and phase portraits.
- Dimension and entropy values of simulated chaotic oscillations agree well with those evaluated from the experiment. For an example, the chaotic time series shown in Figs. 5a and 6a gives a correlation dimension of 1.90 ± 0.02 and a K_2 entropy of $1.8 \pm 0.2\,/\mu\text{s}$; the simulated time series shown in Figs. 5b and 6b gives a correlation dimension of 1.94 ± 0.02 and a K_2 entropy of $1.7 \pm 0.2\,\mu\text{s}$.

Neglecting the effects of radiation trapping and assuming the population in the excited state to be zero, a three dimensional model containing only the (u, v, w)-vector remains, having the light-shift effect as the prominent nonlinear mechanism [5]. Using this model, the chaotic oscillations before the switching to the high transmitting state cannot be simulated. This model shows a narrow range of chaotic behavior in the high transmitting state, where the condition $\partial\,\text{Ay}\,/\partial\varphi < 0$ is valid (see [5]). The scenario thus simulated resembles the one we could observe in the switched-up state.

On the other hand, it is possible to write a three-dimensional model by neglecting the light-shift contribution instead and considering only a transverse magnetic field $\mathbf{\Omega} = \Omega\hat{e}_x$. This three-dimensional model would involve the spin components (v, w) perpendicular to the direction of the magnetic field and the excitation s. This second reduced model shows – for the same values of the parameters – qualitatively the same behavior as the full four-dimensional model. A quantitative reproduction cannot be expected here, since the oscillation frequencies are determined by the absolute value of the magnetic field vector and the neglected longitudinal component is at least of the same magnitude as the transverse component.

5 Conclusion

With a high standard of stabilization reproducible measurements of chaotic scenarios are possible. Exact control of

phase changes reveals a kind of *generalized bistability*, i.e., the coexistence of a fixed point and a periodic or chaotic attractor in a hysteresis loop. A four-dimensional model shows very good agreement with the experiment, regarding signal shapes, frequencies, return maps, attractor dimensions, and entropies. A reduction of the model shows that the mechanism of radiation trapping, though considered here in a very simplified way, is responsible for the chaotic behavior in the parameter range studied here.

References

1. F. Mitschke, R. Deserno, W. Lange, J. Mlynek: Phys. Rev. A **33**, 3219 (1986)
2. J. Nalik, W. Lange, F. Mitschke: Appl. Phys. B **49**, 191 (1989)
3. F. Mitschke, C. Boden, C. Henning, I. Roloff: In *Coherence and Quantum Optics VI*, eds. by J.H. Eberly, L. Mandel, E. Wolf (Plenum, New York 1989) p. 759
4. W. Lange, M. Möller, K. Iwankiw, M. Oestreich, J. Nalik: In *Nonlinear Dynamics in Optical Systems* (Opt. Soc. of Am. Washington DC 1990) pp. FB4-1/439
5. C. Boden, M. Dämmig, F. Mitschke: Phys. Rev. A (in press)
6. T.W. Hänsch, B. Couillaud: Opt. Commun. **35**(3), 441 (1980)
7. J. Nalik, L.M. Hoffer, G.L. Lippi, Ch. Vorgerd, W. Lange: Phys. Rev. A **45**, R4237 (1992)
8. D. Tupa, L.W. Anderson. Phys. Rev. A **36**, 2142 (1987)
9. W. Lange, G. Ankerhold, M. Schiffer, D. Mutschall, T. Scholz: IQEC '92, Digest of Technical Papers
10. P. Grassberger, I. Procaccia: Phys. Rev. Lett. **50**, 346 (1983); Phys. Rev. A **28**, 2591 (1983)
11. M. Möller, W. Lange: To be published